

Design of a Patient-Specific Cranial Phantom (PSCP) for Evaluation Across Multiple Dosimetric Systems in Linac-Based Stereotactic Radiosurgery

Taha Erdoğan*, Duriye Öztürk, Elif Güler Şahin

Department of Radiation Oncology, Afyonkarahisar Health Sciences University, Afyonkarahisar, Turkey

ABSTRACT

In this study, a patient-specific cranial phantom (PSCP) was fabricated using 3D printing technology and its usability in individual quality control processes instead of commercially available 2D/3D phantoms was evaluated. Three patient-specific phantoms (PSCP1, PSCP2 and PSCP3) were modelled using computed tomography (CT) data from three different patients and fabricated using a plant-based biopolymer (STH). RTV2 silicone or paraffin wax were used to represent brain tissue. The quality and dosimetric reliability of the phantoms were analysed using point dose measurements with metal oxide silicon field effect transistor (MOSFET) and beryllium oxide (BeO) dosimetry systems on a Trilogy® radiotherapy machine and compared with treatment planning system (TPS) data. The HU value of neurocranial bones fabricated with 100% infill STH filament was 141 ± 16.7 . Silicone and paraffin wax brain tissue surrogates yielded HU values of 33 ± 6.4 and -56 ± 12.8 , respectively, compared with 22 ± 4.4 for real brain tissue. In MOSFET measurements, dose differences ranged from 0.25% to 7.78%, while BeO dosimetry showed differences between 2.28% and 7.81%. Across both dosimetry systems, S-VMAT plans consistently produced lower measured doses, whereas higher values were observed with M-VMAT. Point dose analysis revealed a statistically significant difference between S-VMAT and M-VMAT techniques for both brain tissue materials, regardless of lesion number ($p < 0.05$), indicating a systematic planning-related effect. The obtained data demonstrate that the PSCP can be used as a mechanically stable and dosimetrically reliable model for patient-specific quality assurance by testing different planning techniques and dosimetry systems.

Keywords: 3D Printer, Silicone, Paraffin Wax, Beryllium Oxide (BeO), Metal Oxide Silicon Field Effect Transistor (MOSFET)

Introduction

Stereotactic radiotherapy (SRS) is a widely preferred method for the treatment of multiple brain metastases (BM) and can be delivered with different dose schedules and treatment techniques. These techniques include conformal dynamic arc, fixed gantry three-dimensional conformal radiotherapy (3DCRT), intensity modulated radiotherapy (IMRT) and volumetric modulated arc therapy (VMAT) (1-5). Currently, VMAT stands out as an advantageous method in the treatment of brain metastases with SRS. The main reason for this is the ability to deliver a precisely shaped three-dimensional (3D) dose distribution over 360 degrees with single or multiple arcs using a dynamic multi-leaf collimator (MLC), variable dose rate and variable gantry motion. However, VMAT is a complex process that requires synchronisation of gantry movement, dose rate

and multi-leaf collimator (MLC) modulation. However, it is known that the accuracy of dose calculation algorithms used in conventional treatment planning systems can decrease in situations involving small field sizes and tissue heterogeneities (6). In order to assess and verify this uncertainty, end-to-end tests should be performed on suitable phantoms. Existing commercial phantoms are typically simple geometric shapes made of solid water equivalent materials and may not be sufficient to accurately reflect clinical scenarios.

In Volumetric Modulated Arc Therapy (VMAT), the radiation dose is applied simultaneously with the dynamic movement of the multileaf collimator (MLC) leaves. This requires synchronisation of dose rate, MLC motion speed and gantry rotation speed. These parameters are controlled by optimisation methods used in the treatment planning system (TPS). Optimisation algorithms

*Corresponding Author: Taha Erdogan, Department of Radiation Oncology, Faculty of Medicine, Afyonkarahisar Health Sciences University, 03200, Afyonkarahisar, Türkiye

E-Mail: taha.erdogan@afsu.edu.tr, GSM: +90 531 792 22 97

ORCID ID: Taha Erdoğan: 0000-0002-3559-8933, Duriye Öztürk: 0000-0002-3265-2797, Elif Güler Şahin: 0000-0002-4150-8711

Received: 07.10.2025, Accepted: 28.03.2026

aim to generate the desired dose distribution by taking into account various factors such as MLC leaf position constraints, dose rates and monitor unit (MU) weights (7,8). However, dose modelling experiments using conventional commercial phantoms may not be reliable enough, especially for small field sizes and in the presence of tissue heterogeneities. This is because these phantoms typically consist of homogeneous and simplified structures and cannot accurately reflect the complex tissue interactions in real clinical scenarios. To overcome this deficiency and create more accurate quality assurance processes, 3D printing technology enables the production of personalised and customisable phantoms. 3D printed phantoms offer more anatomically realistic structures and can mimic tissue heterogeneities with different densities and material compositions. This is a significant advantage in quality assurance for treatments that require high precision, such as stereotactic radiosurgery (SRS). In addition, the use of 3D printed phantoms in patient-based dose verification can improve the accuracy of treatment planning and the reliability of clinical outcomes (9,10). By overcoming the limitations of traditional phantoms, this new approach offers a more effective and flexible solution for quality assurance in modern radiotherapy applications.

3D printing technology, also known as additive manufacturing, plays an important role in the production of phantoms, which are widely used in clinical routine. This technology is particularly beneficial in medical fields such as radiotherapy, where it can be used to create patient-specific models that offer true tissue equivalence. In recent years, there has been increasing interest in the production of phantoms that more realistically replicate patient anatomy and provide high accuracy in terms of tissue equivalence (11,12). Compared to conventional casting techniques, 3D printing offers significant advantages for the production of phantoms used in patient-specific quality assurance (PSQA) processes. Conventional casting techniques are limited to specific shapes and may not adequately reflect complex anatomical structures and heterogeneous tissues. However, 3D printing enables the production of detailed and customisable phantoms based on patient-specific geometry. This increases the accuracy and reliability of personalised quality control processes and offers more flexible solutions for clinical applications. Currently, various methods such as two-dimensional (2D) or three-dimensional (3D) dose reconstruction methods, point dose verification and transmission

dose verification are used in PSQA processes (13). Among these methods, point dose verification is the most widely used method due to its high error sensitivity, ease of use and reliability (14). Point dose verification allows the margin of error to be assessed by comparing the dose values measured in a given region with the dose calculated during treatment planning. It is therefore recognised as an effective method that can both save time and provide accurate results in quality assurance processes. In conclusion, 3D printing technology is making a significant contribution to the development of quality assurance processes in areas that require high precision, such as radiotherapy, thanks to the flexibility and anatomical accuracy it offers in the production of patient-specific phantoms. This innovative manufacturing approach, which overcomes the limitations of traditional methods, enables more reliable, personalised and accurate assessments in clinical applications.

For a phantom to have tissue equivalence, the interaction of the materials used in its manufacture with radiation should have similar properties to human tissue. In this direction, thermoplastic filaments such as polylactic acid (PLA) and acrylonitrile butadiene styrene (ABS) with high filler density (typically 80-90% filler ratio) have been shown to provide successful results in achieving tissue equivalence in terms of dosimetry (14,15). Some works have demonstrated the feasibility of combining 50% gravimetrically measured powdered stone commercial filaments with 50% PLA thermoplastic filament for the replication of bone equivalent density (10,12). However, when using this method, it should be considered that the rock powder content can cause wear on the print nozzle. Therefore, when using high density filaments, nozzles with a diameter of at least 0.6 mm or larger should be preferred. However, the use of larger nozzles may reduce the geometric accuracy that can be achieved in the 3D printing process (10). This suggests that the advantage in terms of tissue equivalence must be balanced against the potential loss in print resolution. In conclusion, these approaches to improving tissue equivalence expand the potential for the use of 3D printing technology in medical physics and radiotherapy applications, but require careful consideration of the balance between material selection, printing parameters and geometric accuracy. In the future, the development of new generation filaments that are wear resistant and compatible with thinner

nozzles may contribute to the wider use of this technology in clinical applications.

In contrast to quality assurance (QA) phantoms produced using standard casting techniques, this study investigated the design, manufacturing process and adaptability to clinical routines of a patient-specific cranial phantom (PSCP) produced using 3D printing technology for use in patient-specific quality assurance (PSQA) testing. The aim was to evaluate the PSCP in terms of anatomical accuracy, material properties and dosimetry, and to investigate in detail the potential advantages over conventional methods. Thanks to the flexibility of 3D printing technology, it has become possible to produce phantoms suitable for individual patient anatomy and integrate them into clinical applications, thus enabling more accurate and reliable quality assurance processes.

Materials and Methods

Modeling of Patient-Specific Cranial Phantom (PSCP): In this study, Digital Imaging and Communication in Medicine (DICOM) files of patients diagnosed with multiple brain metastases (BM) were analysed to develop a patient-specific cranial phantom (PSCP). Three patients with three, four, and five metastases from different primary cancers who were previously treated at Afyonkarahisar University of Health Sciences, Faculty of Medicine, Department of Radiation Oncology between October 2019 and April 2020 were selected. The maximum diameter of metastatic lesions in these patients was limited to 4 cm. To generate the PSCP, computed tomography (CT) simulation data obtained during initial treatment planning with a slice thickness of 1 mm were used. The CT images of the selected BM patient were examined and three different phantom models were designed using individualised patient data. The DICOM files were imported into MIMICS v.19 software (Materialise, Leuven, Belgium), where the neurocranium, paranasal sinus and skull structure were reconstructed to develop an anatomically accurate model. The fundamental objective was to generate a fully personalised phantom without modifying the patient's original bone structures (Figure 1). Once the digital model was finalised, it was converted to STL format to make it compatible with 3D printing technology. The workflow diagram illustrating the 3D anatomical digital modelling process is shown in Figure 2, systematically detailing each step of the custom phantom fabrication process. This approach

enhances patient-specific quality assurance (PSQA) by providing an accurate anatomical reference, facilitating smoother integration into clinical practice.

Development of a PSCP-Based, Tissue-Equivalent Cranial Phantom Using 3D Printing: The Hounsfield Unit (HU) value of bone tissue varies with age and anatomical location. In this study, the selected patients had an average age of 62.6 years. STH filament, a plant-based biopolymer with a specific gravity of 1.22 g/cm³, was used for the fabrication of neurocranial bone and body structure due to its favourable mechanical properties. The PSCP was fabricated using the Combined Stacking Modelling (CSM) technique on a Diamond DT3X 3D printer (Figure 3/a,b) with a nozzle diameter of 400 µm and a resolution optimised for precision. Printing was performed at 218°C with a tray temperature of 80°C. The final model was completed in 16 hours at a print head speed of 40 mm/s. The structure was reinforced with a 300 µm thick outer shell and a fully compact inner fill for increased durability. The PSCP consists of two primary structural components: brain tissue fabricated using RTV2 silicone or paraffin wax, and a body shell designed to accommodate the neurocranium bone. The brain structure was created by preparing RTV2 silicone and casting it into a neurocranium bone mould (Figure 3/c). To ensure proper moulding, the silicone and catalyst were mixed in precise proportions until homogeneous. A mould release spray was applied to prevent sticking, and the mixture was carefully poured from a single point at a steady rate to minimise air pockets. The material was then allowed to solidify at room temperature for 24 hours. After completion of the dosimetric measurements with the silicone-based brain tissue, the mould was cleaned and the same process was repeated with melted paraffin wax (Figure 3/d). The wax was allowed to solidify under identical conditions, requiring an additional 24 hours of drying (Figure 3/e).

Radiological assessment of the PSCP: The Hounsfield Unit (HU) values of the patient's neurocranial bones and brain tissue were analysed and compared with the HU values of the materials used in the phantom fabrication to assess their radiological equivalence. Basic plan dose verification with MOSFET and BeO dosimeters. As a final step, all phantoms were used in treatment irradiations of real patients treatment plan.

Evaluation of PSCP Dosimetric Quality Assurance (QA): PSCP experiments have been performed for the development, evaluation, and validation of SRS techniques and optimization of imaging parameters. Clinical feasibility of PSCP was evaluated using each patient's actual treatment plans. The patient was immobilised in the supine position with a thermoplastic mask providing anterior and posterior cranial support. CT scans were acquired on a Toshiba Aquilion LB (Toshiba® Medical Systems, Otowara, Japan) at 1 mm slice thickness without contrast. The CT images were fused with T1 contrast-enhanced MR images at 1.5 mm intervals for treatment planning. A radiation oncologist delineated the gross tumour volume (GTV) and organs at risk (OAR) based on the MRI. A planning target volume (PTV) was created by adding a 2 mm isotropic margin to the GTV. Dose prescriptions followed the Radiation Therapy Oncology Group (RTOG) 90-05 guidelines: 24 Gy for lesions < 20 mm, 18 Gy for 21-30 mm, and 15 Gy for 31-40 mm in diameter (16), while OAR limits followed QUANTEC recommendations. Single-isocentre (S-VMAT) (Figure 4/a) and multi-isocentre (M-VMAT) (Figure 4/b). VMAT-based stereotactic radiosurgery (SRS) treatment plans were generated using Eclipse® TPS v13.6 with 6 MV photon beams on a Trilogy linear accelerator (Varian Medical Systems, Palo Alto, CA, USA). The isocentre for S-VMAT was placed at the geometric centre of the PTV, while M-VMAT plans used dual isocenters, each positioned at the centre of the entire PTV on each side. Plans were optimised using a Millennium MLC, a dose rate of 600 MU/min and doses of either 400 cGy or 300 cGy in a single fraction. Dose calculations were performed using the Analytical Anisotropic Algorithm (AAA) v13.7 with a 2.5 mm dose grid. According to the clinical protocol, 95% of the prescribed dose covered at least 100% of the PTV, while avoiding exceeding 110%. The primary goal was to achieve highly conformal dose distributions while minimising OAR exposure. All treatment plans were generated using the clinical TPS (Varian® Medical Systems, Palo Alto, CA, USA). To evaluate the PSCP for use in treatment QA control tests; each phantom design was irradiated 6 times using two different plans (S-VMAT and M-VMAT). In the whole study, a total of 36 irradiations were performed. Each dosimetric measurement was repeated 6 times per phantom and plan. Since the lifetime of MOSFET dosimeters is limited, the prescription dose was planned as 400cGy.

Statistical Analysis: Statistical analysis was performed to explore the agreement and relative differences between treatment planning system (TPS) calculated doses and point dose measurements obtained using MOSFET and BeO dosimeters. Since dose measurements were obtained from the same phantom, planning target volume (PTV), and treatment plan, paired comparisons were conducted. Data normality was assessed using the Shapiro-Wilk test. Since the study design involved repeated measurements across multiple variables (phantom models, tissue-equivalent materials, and planning techniques) and the data did not follow a normal distribution, non-parametric tests were employed. The Friedman test was used to determine whether there were statistically significant differences between the multiple dependent groups (Silicone S-VMAT, Silicone M-VMAT, Paraffin S-VMAT, and Paraffin M-VMAT). For subsequent pairwise comparisons (post-hoc analysis), the Wilcoxon signed-rank test with a Bonferroni correction was applied to identify specific differences between tissue types and planning techniques. All statistical analyses were performed using SPSS software (v19.0, IBM Corp., Armonk, NY, USA), and a p-value of less than 0.05 was considered statistically significant.

Ethical Approval: This study was conducted with the approval of the Non-Interventional Clinical Research Ethics Committee of Afyonkarahisar Health Science University Faculty of Medicine (decision number: 2020/02, dated: 07.02.2020)

Results

Radiological Assessment of The PSCP: HU evaluation of the PSCP models was performed using images acquired with a 120 kV cranial imaging protocol (1 mm slice thickness). Hounsfield Unit (HU) values of the neurocranium and brain tissue were measured at 15 different locations, and the mean and standard deviation were calculated. All measurements were conducted with the PSCP models positioned under a thermoplastic mask (Figure 5). The neurocranial bones printed with STH filament at 100% infill showed an average HU value of 141 ± 16.7 . For brain tissue simulation, silicone and paraffin wax yielded HU values of 33 ± 6.4 and -56 ± 12.8 , respectively, whereas the corresponding HU value measured in patient brain tissue was 22 ± 4.4 .

Basic Plan Dose Verification With MOSFET and BeO Dosimeters: All measurements were taken consecutively without moving the MOSFET dosimeters. In BeO irradiations, 3 dosimeters were placed at the point where each measurement was to be taken and the measurements were

Table 1: BeO and MOSFET dosimetry Results Obtained After S-VMAT and M-VMAT SRS Irradiation of PSCP 1 Using Silicone As Brain Tissue

PSCP 1 (Brain Tissue: Silicone)	PTV 1 (PD: 250 cGy)	PTV 2 (PD: 300 cGy)	PTV 3 (PD: 400 cGy)
S-VMAT (TD)	269.35	313.15	415.05
BeO (AverageDose \pm SD)	289.08 \pm 7.52	336.77 \pm 11.04	424.87 \pm 8.04
MOSFET (AverageDose \pm SD)	283.97 \pm 1.02	326.22 \pm 3.12	418.77 \pm 0.86
M-VMAT (TD)	277.80	319.40	422.25
BeO (AverageDose \pm SD)	287.49 \pm 4.55	330.14 \pm 6.62	444.24 \pm 7.34
MOSFET (AverageDose \pm SD)	279.87 \pm 0.92	324.36 \pm 1.30	433.14 \pm 0.80

TD: Treatment Plan Maksimum Dose, SD: Standard Deviation, PD: Prescription Dose

Table 2: Percent Difference Between Treatment Planning Doses BeO and MOSFET Dosimetry Results Obtained From PSCP 1 Using Silicone As Brain Tissue

PSCP 1 (Brain Tissue: Silicone)	PTV 1 (PD: 250 cGy)	PTV 2 (PD: 300 cGy)	PTV 3 (PD: 400 cGy)
S-VMAT			
BeO (AverageDose)	7.33%	7.54 %	2.36%
MOSFET (AverageDose)	5.43%	4.17%	0.90%
p	0.01	0.00	0.00
M-VMAT			
BeO (AverageDose)	3.48%	3.36%	5.21%
MOSFET (AverageDose)	0.75%	1.55%	2.58%
p	0.07	0.23	0.18

PD: Prescription Dose

Table 3: BeO and MOSFET Dosimetry Results Obtained After S-VMAT and M-VMAT SRS Irradiation of PSCP 1 Using Paraffin Wax As Brain Tissue

PSCP 1 (Brain Tissue: Paraffinwax)	PTV 1 (PD: 250 cGy)	PTV 2 (PD: 300 cGy)	PTV 3 (PD: 400 cGy)
S-VMAT (TD)	269.35	313.15	415.05
BeO (AverageDose \pm SD)	288.52 \pm 12.21	337.12 \pm 14.85	436.24 \pm 8.42
MOSFET (AverageDose \pm SD)	284.22 \pm 2.65	328.24 \pm 2.01	424.02 \pm 1.98
M-VMAT (TD)	277.82	319.40	422.25
BeO (AverageDose \pm SD)	292.08 \pm 13.48	338.86 \pm 9.76	454.28 \pm 5.10
MOSFET (AverageDose \pm SD)	288.54 \pm 2.21	327.55 \pm 1.48	439.42 \pm 1.78

TD: Treatment Plan Maksimum Dose, SD: Standard Deviation, PD: Prescription Dose

Table 4: Percent Difference Between Treatment Planning Doses BeO and MOSFET Dosimetry Results Obtained From PSCP 1 Using Paraffin Wax As Brain Tissue

PSCP 1 (Brain Tissue: Paraffinwax)	PTV 1 (PD: 250 cGy)	PTV 2 (PD: 300 cGy)	PTV 3 (PD: 400 cGy)
S-VMAT			
BeO (AverageDose)	7.12%	7.65%	5.11%
MOSFET (AverageDose)	5.52%	4.82%	2.16%
p	0.00	0.03	0.01
M-VMAT			
BeO (AverageDose)	5.13%	6.09%	7.58%
MOSFET (AverageDose)	3.86%	2.55%	4.06%
p	0.08	0.85	0.66

PD: Prescription Dose

Table 5: BeO and MOSFET Dosimetry Results Obtained After S-VMAT and M-VMAT SRS Irradiation of PSCP 2 Using Silicone As Braintissue

PSCP 2 (Brain Tissue: Silicone)	PTV 1 (PD: 400 cGy)	PTV 2 (PD: 300 cGy)	PTV 3 (PD: 400 cGy)	PTV 4 (PD: 400 cGy)
S-VMAT (TD)	431.25	328.00	411.45	443.27
BeO (AverageDose ± SD)	461.73 ±16.62	344.83 ±18.01	440.67 ±18.44	477.73 ±22.31
MOSFET (AverageDose ± SD)	444.17 ±2.58	328.83 ±2.80	422.27 ±2.74	460.3 ±3.04
M-VMAT (TD)	436.75	317.25	418.10	444.04
BeO (AverageDose ± SD)	451.72 ±13.44	342.03 ±10.50	444.83 ±13.36	478.28 ±18.96
MOSFET (AverageDose ± SD)	445.53 ±1.54	321.57 ±1.48	425.90 ±2.02	451.43 ±1.45

TD: Treatment Plan Maksimum Dose, SD: Standard Deviation, PD: Prescription Dose

Table 6: Percent Difference Between Treatment Planning Doses BeO and MOSFET Dosimetry Results Obtained From PSCP 2 Using Parafin Wax As Brain Tissue

PSCP2 (Brain Tissue: Silicone)	PTV 1 (PD: 250 cGy)	PTV 2 (PD: 300 cGy)	PTV 3 (PD: 400 cGy)	PTV 4 (PD: 400 cGy)
S-VMAT				
BeO (AverageDose)	7.08%	5.13%	7.10%	7.77%
MOSFET (AverageDose)	3.00%	0.25%	2.63%	3.84%
p	0.01	0.05	0.01	0.02
M-VMAT				
BeO (AverageDose)	3.43%	7.81%	6.39%	7.71%
MOSFET (AverageDose)	2.01%	1.36%	1.87%	1.66%
p	0.45	0.31	0.18	0.06

PD: Prescription Dose

Table 7: BeO and MOSFET Dosimetry Results Obtained After S-VMAT and M-VMAT SRS Irradiation of PSCP 2 Using Parafin Wax As Brain Tissue

PSCP 2 (Brain Tissue: Paraffinwax)	PTV 1 (PD: 400 cGy)	PTV 2 (PD: 300 cGy)	PTV 3 (PD: 400 cGy)	PTV 4 (PD: 400 cGy)
S-VMAT (TD)	431.25	328.00	411.45	443.27
BeO (AverageDose ± SD)	453.45±35.06	348.62±22.48	436.82±21.03	462.10±27.83
MOSFET (AverageDose ± SD)	442.99±5.13	334.03±2.06	428.50 ±3.88	441.52±4.10
M-VMAT (TD)	436.75	317.25	418.10	444.04
BeO (AverageDose ± SD)	458.40±19.42	338.12±16.55	443.47±13.92	471.12 ±22.13
MOSFET (AverageDose ± SD)	453.51±2.45	341.92±1.82	434.40±2.34	463.71 ±2.70

TD: Treatment Plan Maksimum Dose, SD: Standard Deviation, PD: Prescription Dose

averaged. In this way, it was aimed to prevent setup uncertainties and only the uncertainties of the dosimeters were aimed to affect the measurement results. The BeO dosimeters and MOSFET dosimeters were impoted in PTVs. In each irradiation, BeO dosimeters and MOSFET dosimeters were placed inside the PTVs

independently of each other. Then, initial position control was performed with portal images in AP and LAT directions. And then, the positions of the PSCP were checked with CBCT images in the whole axis (Figure 6). Images from planning and PTV contours were used to determine the accuracy of dosimetry positions. All detailed

Table 8: Percent Difference Between Treatment Planning Doses BeO and MOSFET Dosimetry Results Obtained From PSCP 2 Using Paraffin Wax As Brain Tissue

PSCP2 (Brain Tissue: Paraffinwax)	PTV 1 (PD: 250 cGy)	PTV 2 (PD: 300 cGy)	PTV 3 (PD: 400 cGy)	PTV 4 (PD: 400 cGy)
S-VMAT				
BeO(AverageDose)	5.15%	6.29%	6.17%	4.25%
MOSFET (AverageDose)	2.72%	1.84%	4.14%	0.39%
p	0.02	0.05	0.03	0.00
M-VMAT				
BeO (AverageDose)	4.96%	6.58%	6.10%	6.10%
MOSFET (AverageDose)	3.84%	7.78%	3.90%	4.43%
p	0.51	0.33	0.78	0.08

PD: Prescription Dose

Table 9: BeO and MOSFET Dosimetry Results Obtained After S-VMAT and M-VMAT SRS Irradiation of PSCP 3 Using Silicone As Brain Tissue

PSCP 3 (Brain Tissue: Silicone)	PTV 1 (PD: 400 cGy)	PTV 2 (PD: 300 cGy)	PTV 3 (PD: 400 cGy)	PTV 4 (PD: 400 cGy)	PTV 5 (PD: 400 cGy)
S-VMAT (TD)	418.75	422.05	418.00	419.85	415.55
BeO (AverageDose ± SD)	443.47 ±32.06	431.67 ±27.13	442.17 ± 12.06	438.43 ±11.48	435.47 ±22.16
MOSFET (AverageDose ± SD)	425.80 ±4.17	427.33 ±2.02	422.27 ±5.41	427.31 ±8.54	427.90 ±2.48
M-VMAT (TD)	450.33	428.40	416.35	418.75	428.20
BeO (AverageDose ± SD)	472.79 ±25.56	455.88 ±28.32	443.63 ± 12.88	446.03 ±16.08	458.77 ± 17.30
MOSFET (AverageDose ± SD)	463.44 ±4.16	439.86 ±2.22	431.33 ±3.38	431.16 ±3.01	445.50 ±3.55

TD: Treatment Plan Maksimum Dose, SD: Standard Deviation, PD: Prescription Dose

Table 10: Percent Difference Between Treatment Planning Doses BeO and MOSFET Dosimetry Results Obtained From PSCP 3 Using Silicone As Brain Tissue

PSCP3 (Brain Tissue: Silicone)	PTV 1 (PD: 250 cGy)	PTV 2 (PD: 300 cGy)	PTV 3 (PD: 400 cGy)	PTV 4 (PD: 400 cGy)	PTV 5 (PD: 400 cGy)
S-VMAT					
BeO (AverageDose)	5.90%	2.28%	5.78%	4.43%	4.79%
MOSFET (AverageDose)	1.68%	1.25%	1.02%	1.79%	3.00%
p	0.01	0.01	0.03	0.00	0.01
M-VMAT					
BeO (AverageDose)	4.98%	6.41%	6.55%	6.51%	7.14%
MOSFET (AverageDose)	2.91%	2.68%	3.60%	2.96%	4.04%
p	0.38	0.07	0.47	0.12	0.41

PD: Prescription Dose

Table 11: BeO and MOSFET Dosimetry Results Obtained After S-VMAT and M-VMAT SRS Irradiation of PSCP 3 Using Paraffin Wax As Brain Tissue

PSCP 3 (Brain Tissue: Paraffinwax)	PTV 1 (PD: 400 cGy)	PTV 2 (PD: 300 cGy)	PTV 3 (PD: 400 cGy)	PTV 4 (PD: 400 cGy)	PTV 5 (PD: 400 cGy)
S-VMAT (TD)	418.75	422.05	418.00	419.85	415.55
BeO (AverageDose ± SD)	442.05 ±17.45	446.22 ± 34.02	437.11 ± 21.89	441.01 ± 22.18	432.28 ± 37.50
MOSFET (AverageDose ± SD)	435.22 ± 2.49	438.81 ± 2.49	434.47 ±3.01	437.77 ± 3.18	437.90 ±1.23
M-VMAT (TD)	450.33	428.40	416.35	418.75	428.20
BeO (AverageDose ± SD)	476.21 ±30.16	453.82 ±41.07	446.22 ±27.03	448.61 ±22.56	459.08 ±15.15
MOSFET (AverageDose ± SD)	458.13 ±3.25	437.79 ±2.56	431.27 ±1.19	436.66 ±1.48	441.25 ±2.01

TD: Treatment Plan Maksimum Dose, SD: Standard Deviation, PD: Prescription Dose

Table 12: Percent Difference Between Treatment Planning Doses BeO and MOSFET Dosimetry Results Obtained From PSCP 3 Using Paraffin Wax As Brain Tissue

PSCP3 (Brain Tissue: Paraffinwax)	Tissue:	PTV 1 (PD: 250 cGy)	PTV 2 (PD: 300 cGy)	PTV 3 (PD: 400 cGy)	PTV 4 (PD: 400 cGy)	PTV 5 (PD: 400 cGy)
			S-VMAT			
BeO (AverageDose)		5.56%	5.72%	4.57%	5.04%	4.03%
MOSFET (AverageDose)		3.93%	3.97%	3.94%	4.27%	5.86%
p		0.04	0.00	0.01	0.00	0.02
			M-VMAT			
BeO (AverageDose)		5.75%	5.93%	7.17%	7.13%	7.21%
MOSFET (AverageDose)		1.73%	2.19%	3.58%	4.28%	3.05%
p		0.05	0.22	0.10	0.07	0.36

PD: Prescription Dose

measurement results and individual dosimetric data regarding each phantom (PSCP1, PSCP2, PSCP3), tissue material, and planning technique examined within the scope of the study are presented in Tables 1-12. A general evaluation of these tables, including statistical interaction analyses and a collective summary of the study parameters, is provided in Table 13.

Discussion

The Patient-Specific Cranial Phantom (PSCP) was designed to replicate patient-specific cranial anatomy with high geometric and radiological accuracy by incorporating anthropomorphic components that realistically represent the human skull and intracranial structures. Compared with conventional phantom designs reported in the literature, the PSCP provides a

more detailed representation of bone anatomy, brain tissue equivalence, and overall anatomical geometry. This study was developed to address existing limitations in phantom design, particularly for stereotactic radiosurgery (SRS) quality assurance (QA) applications, and to evaluate the dosimetric performance of the PSCP under clinically relevant conditions. Figure 4 presents the 3D-printed PSCP alongside a commercial anthropomorphic head phantom. To ensure mechanical stability without inducing unwanted rotational motion, the shell thickness was standardized to 2 mm in all directions. Cone-beam computed tomography (CBCT) imaging confirmed the absence of rotational displacement during setup.

To evaluate the radiological properties of the PSCP, Hounsfield Unit (HU) values of the neurocranial bone and brain tissue regions were measured at 25

Table 13: The Impact of Planning Techniques and Tissue-Equivalent Materials on Dosimetric Performance: A Comparative Interaction Analysis

Dosimetry System	Experimental Group	Mean Error % (\pm SD)	Friedman χ^2	p-value (Overall)	Post-hoc Significance
MOSFET	S-VMAT + Silicone	2.11 \pm 1.2	18.45	< 0.001	S-VMAT vs. M-VMAT
	M-VMAT + Silicone	2.31 \pm 0.9			
	S-VMAT + Paraffin	3.61 \pm 1.5			Silicone vs. Paraffin
	M-VMAT + Paraffin	3.93 \pm 1.8			
BeO	S-VMAT + Silicone	5.53 \pm 1.8	12.12	7	S-VMAT vs. M-VMAT
	M-VMAT + Silicone	5.91 \pm 1.4			
	S-VMAT + Paraffin	5.73 \pm 1.1			(Non-significant)
	M-VMAT + Paraffin	6.24 \pm 0.8			

SD: Standard Deviation; S-VMAT: Single-Arc Volumetric Modulated Arc Therapy; M-VMAT: Multi-Arc Volumetric Modulated Arc Therapy; BeO: Beryllium Oxide; MOSFET: Metal Oxide Silicon Field Effect Transistor. Statistical significance was determined using the Friedman test ($p < 0.05$)

different locations on CT images. Soft tissues were characterized within a HU range of -500 to 200 , while bone structures exhibited HU values above 200 , consistent with the known attenuation properties of human tissues (17,18). HU values reported in the literature for different bone types range between 50 and 3000 (19). In a previous study, an anthropomorphic head phantom fabricated using fused deposition modeling (FDM) with acrylonitrile butadiene styrene (ABS) material exhibited an average HU value of -339 , indicating limited capability to replicate human tissue density variations (7). To overcome this limitation, the PSCP was fabricated using STH filament, achieving a neurocranial HU value of 141 ± 16.7 at 100% infill density. Despite full infill, the measured HU values remained lower than expected, likely due to the intrinsic internal structure of 3D-printed materials. Although bone structures have been reported to influence dosimetry, previous studies demonstrated no clinically significant dose differences between anthropomorphic and 3D-printed phantoms (17). For soft tissue equivalence, paraffin wax and silicone were selected for brain tissue modeling based on their reported radiological properties. Paraffin wax has been previously reported to exhibit a HU value of approximately -74 with a relative electron density of 0.926 (19). In the present study, the measured HU values of silicone and paraffin wax were 33 ± 6.4 and -56 ± 12.8 , respectively. These findings indicate that silicone provides a closer approximation to the HU

characteristics of real brain tissue and therefore offers improved radiological equivalence.

Dosimetric evaluation was performed by comparing doses calculated by the treatment planning system (TPS) with measured point doses. In the first phase, the performance of the MOSFET and beryllium oxide (BeO) dosimeters was assessed (Tables 1–12). Tissue equivalence is particularly important when dosimeters are placed directly on a phantom or patient and dose distributions are analyzed (20). BeO dosimeters, with an effective atomic number of 7.2 , exhibit closer tissue equivalence than other optically stimulated luminescence (OSL) materials and were therefore selected as the primary dosimetry system, while MOSFET was used as a complementary system (21). Analysis of MOSFET measurements revealed that the lowest percentage difference between planned and measured doses was 0.25% for PSCP2 (Table 6). A statistically significant difference was observed between S-VMAT and M-VMAT plans, indicating a systematic trend in point dose measurements ($p = 0.01$). The highest percentage difference observed using MOSFET was 7.78% for PSCP2 (Table 8); however, no statistically significant difference was found between S-VMAT and M-VMAT plans for this case ($p = 0.33$). BeO dosimeter measurements showed the lowest percentage difference of 2.28% for PSCP3 (Table 10) and the highest difference of 7.81% for PSCP2 (Table 6). Due to the repeated-measurement nature of the study,

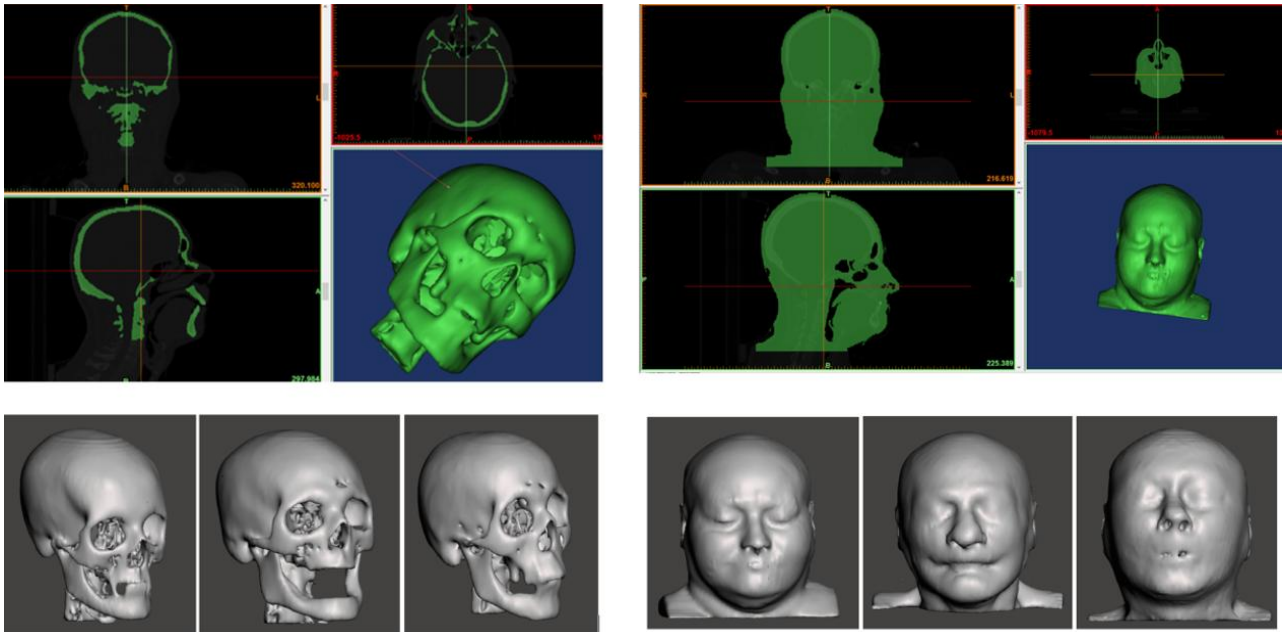


Fig. 1. Three different phantom models were created using each patient's own DICOM data

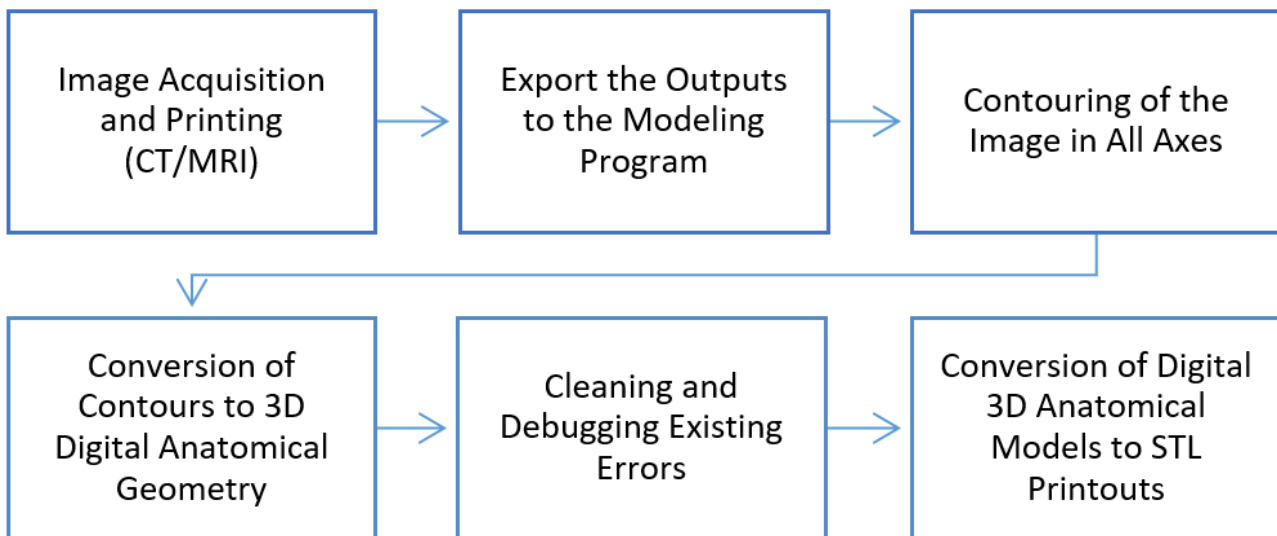


Fig. 2. The Workflow Chart of The Digital 3D Anatomical Modeling Process

statistically significant findings were interpreted as indicative of systematic trends rather than definitive inferential outcomes. Across both dosimetry systems, consistently lower measured dose values were observed for S-VMAT plans, whereas higher dose values were obtained for M-VMAT plans ($p < 0.05$). This systematic pattern is likely associated with field size variability (23,24). The reduced average field size in S-VMAT plans decreases low-energy scatter within the PSCP, thereby affecting dosimeter response. Consequently, the field size correction factor proposed by Mizuno et al. may improve the accuracy of S-VMAT plan verification (21). In contrast, the overlap of dose distributions from multiple isocenters in M-VMAT plans contributes to increased maximum

dose values. Comparison of BeO and MOSFET measurements demonstrated that MOSFET dosimetry consistently yielded smaller percentage differences relative to planned PTV doses, along with lower standard deviation values. These findings suggest that MOSFET dosimetry offers higher reproducibility and accuracy for plan verification procedures. Consistent with previous reports, the influence of bone structures on dosimetry did not result in significant dose differences between anthropomorphic head phantoms and 3D-printed phantoms (25,26). Accordingly, the contribution of brain tissue equivalence to dosimetric accuracy was examined in detail during the final phase of the study. When paraffin-based brain tissue measurements were

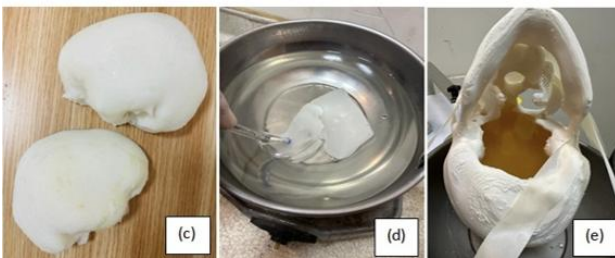


Fig. 3. The anatomical model containing PSCP (the neurocranium bone and body shell), (a,b) PSCP output was $145 \times 160 \times 205 \text{ mm}^3$ and printing time was completed in 16 h., (c) The neurocranium bone was filled with using RTV2 silicone., (d,e) melted paraffin wax brain tissue and 24 hours were waited for the melted paraffin wax to freeze

compared with TPS data, the highest and lowest percentage differences (7.78% and 0.39%, respectively) were both observed for PSCP2. Similarly, silicone-based brain tissue measurements yielded the highest (7.81%) and lowest (0.25%) percentage differences for PSCP2. These findings indicate that the magnitude of percentage differences depends not only on phantom configuration but also on measurement location and planning technique.

Evaluation of the summary data presented in Table 13 demonstrates that patient-specific phantoms produced using 3D printing can serve as accurate alternatives to commercial phantoms in SRS quality control procedures. Friedman test analysis confirmed that the dosimetric differences between experimental groups were statistically significant ($p < 0.001$). Comparable reliability levels were observed across all three phantom models (PSCP1, PSCP2, and PSCP3), with silicone-based brain tissue models exhibiting statistically superior tissue equivalence and improved agreement between measured and calculated doses. Regarding planning techniques, the systematic deviations observed in S-VMAT plans (2.11%–5.73%) are attributed to small-field dosimetric challenges and volume-averaging effects inherent to

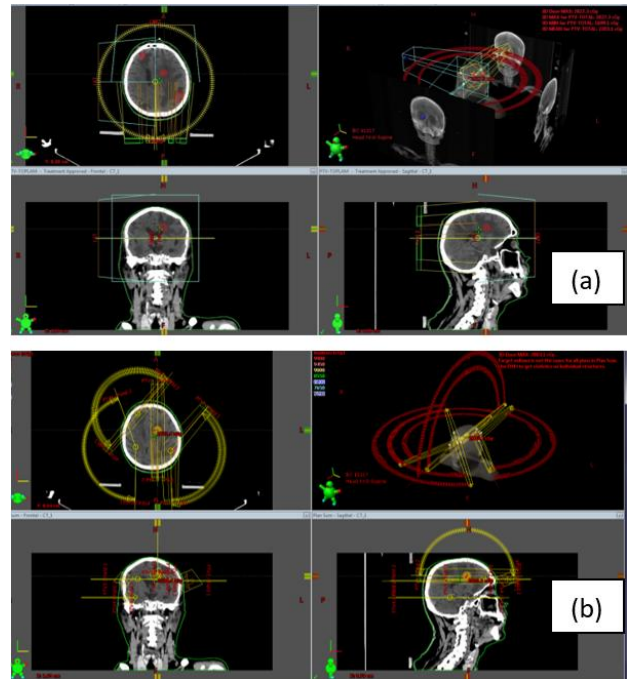


Fig. 4. (a) The single (S-VMAT) isocenter arc VMAT SRS treatment plans.(b) The multiple (M-VMAT) isocenter arc VMAT SRS treatment plans

SRS (31). In contrast, the higher agreement achieved with M-VMAT plans suggests that multiple arc angles mitigate setup uncertainties and heterogeneity calculation risks.

This study has several limitations. First, the PSCP models were developed and evaluated using a limited number of patient datasets, which may restrict the generalizability of the findings to broader patient populations with varying cranial anatomies and tissue heterogeneities. Second, although high infill densities were used, the 3D printing materials and fabrication techniques could not fully replicate the complete density spectrum of human bone tissue, as reflected by the lower-than-expected HU values for the neurocranium. This limitation is inherent to current 3D printing technologies and material microstructures. In addition, the dosimetric evaluation was based on point dose measurements, which do not fully capture three-dimensional dose distributions. This limitation is particularly relevant for SRS applications characterized by steep dose gradients, where point measurements are sensitive to positioning uncertainties and small-field effects. Although repeated measurements and the use of two independent dosimetry systems partially mitigated these effects, volumetric dosimetric methods could provide complementary information. Finally, the analysis was performed using a single treatment planning system and a limited set of planning techniques (S-VMAT and M-VMAT). Future studies

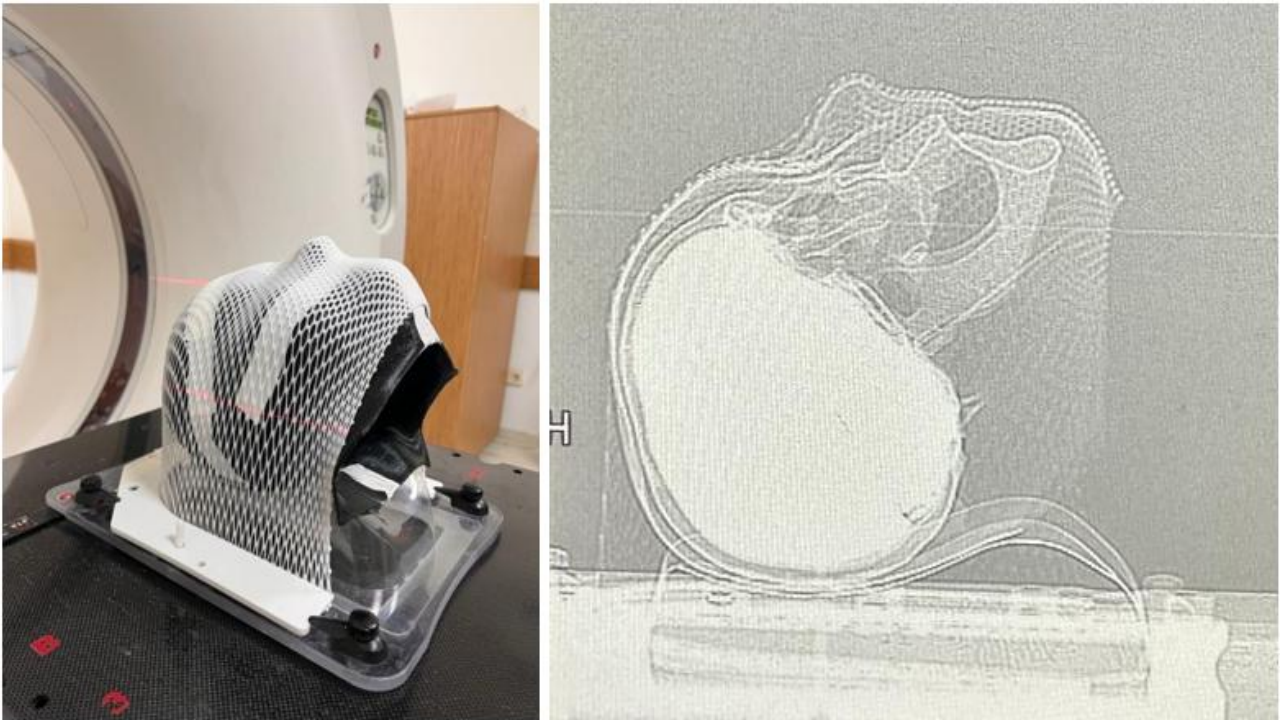


Fig. 5. CT imaging of PSCP Using Clinical Protocols

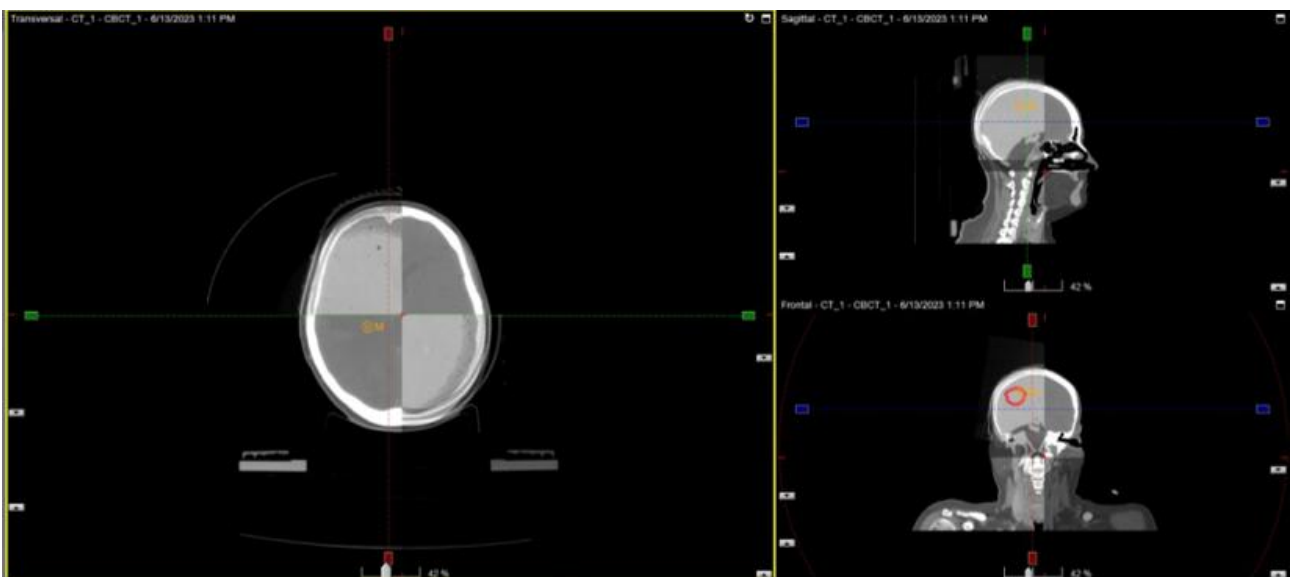


Fig. 6. The Positions of the PSCP Were Checked With CBCT Images in the Whole Axis

incorporating different dose calculation algorithms, beam energies, and planning systems would further strengthen the clinical applicability and generalizability of the PSCP.

A patient-specific cranial phantom (PSCP) was developed using a low-cost personal 3D printer with STH filament in this study. The PSCP was designed to replicate brain tissue equivalence and ensure compatibility with X-ray imaging for both anatomical visualisation and dosimetric evaluation. Its clinical applicability has been validated using

various treatment planning techniques and dosimetry systems. This study is unique in the literature due to its patient-specific geometry, the use of a plant-based STH polymer filament and the incorporation of different brain tissue materials. In contrast to standard QA phantoms produced by casting methods, the PSCP demonstrated acceptable geometric accuracy and cost efficiency. However, the manufacturing process needs to be improved, as the total printing time was approximately 16 hours. Radiotherapy

departments using this method can produce customised PSCPs to their own QA requirements.

References

1. Leksell L. The stereotaxic method and radiosurgery of the brain. *Acta Chir Scand* 1951; 102: 316-319.
2. Hakim R, Alexander E III, Loeffler JS, Shrieve DC, Wen P, Fallon MP, et al. Results of linear accelerator-based radiosurgery for intracranial metastases. *Neurosurgery* 1998; 42: 446-453.
3. Sarkar B, Pradhan A, Munshi A. Dosimetric evaluation of different parameters for small field radiosurgery using Monte Carlo simulation. *Indian J Cancer* 2016; 53: 166-173.
4. Oliver M, Gagne I, Bush K, Zavgorodni S, Ansbacher W, Beckham W. Clinical comparison of helical tomotherapy and IMRT planning for head and neck cancer. *Radiother Oncol* 2010; 97: 554-560.
5. Peng J, Zhang Z, Zhou L, Zhao J, Wang J, Kong L, et al. Evaluation of different planning techniques for total scalp irradiation using 3D conformal radiotherapy and IMRT. *Med Phys* 2013; 40: 031703.
6. Halvorsen PH, Cirino E, Das IJ, Garrett JA, Yang J, Yin FF, et al. AAPM-RSS medical physics practice guideline 9.a for SRS-SBRT. *J Appl Clin Med Phys* 2017; 18: 10-21.
7. Yea JW, Park JW, Kim SK, Kim DY, Kim JG, Seo CY, et al. Feasibility of a 3D-printed anthropomorphic patient-specific head phantom for patient-specific quality assurance of intensity-modulated radiotherapy. *PLoS One* 2017; 12: e0181560.
8. Tatsumi D, Hosono MN, Nakada R, Ishii K, Tsutsumi S, Inoue M, et al. Direct impact analysis of multi-leaf collimator leaf position errors on dose distributions in volumetric modulated arc therapy. *Phys Med Biol* 2011; 56: 237-246.
9. Tino R, Leary M, Yeo A, Kyriakou E, Kron T, Brandt M. Additive manufacturing in radiation oncology: a review of clinical practice, emerging trends and research opportunities. *Int J Extrem Manuf* 2020; 2: 012003.
10. Kairn T, Peet S, Yu L, Crowe S. Long-term reliability of optically stimulated luminescence dosimeters. *World Congr Med Phys Biomed Eng* 2018; 68: 561-564.
11. Leary M, Kron T, Keller C, Franich R, Lonski P, Subic A. Additive manufacture of custom radiation dosimetry phantoms. *Mater Des* 2015; 86: 487-499.
12. Okkalidis N, Marinakis G. Accurate replication of soft and bone tissues with 3D printing. *Med Phys* 2020; 47: 2206-2211.
13. Dong L, Antolak J, Salehpour M, Forster K, O'Neill L, Kendall R, et al. Patient-specific point dose measurement for IMRT monitor unit verification. *Int J Radiat Oncol Biol Phys* 2003; 56: 867-877.
14. Van der Walt M, Crabtree T, Albantow C. PLA as a suitable 3D printing thermoplastic for use in external beam radiotherapy. *Australas Phys Eng Sci Med* 2019; 42: 1165-1176.
15. Hamedani BA, Melvin A, Vaheesan K, Gadani S, Pereira K, Hall AF. Three-dimensional printing CT-derived objects with controllable radiopacity. *J Appl Clin Med Phys* 2018; 19: 317-328.
16. Shaw E, Scott C, Souhami L, Dinapoli R, Kline R, Farnan N. Single dose radiosurgical treatment of recurrent primary brain tumors and brain metastases. *Int J Radiat Oncol Biol Phys* 2000; 47: 291-298.
17. Kamomae T, Shimizu H, Nakaya T, Okudaira K, Aoyama T, Oguchi H, et al. Three-dimensional printer-generated patient-specific phantom for artificial in vivo dosimetry. *Phys Med* 2017; 44: 205-211.
18. Park JW, Oh SA, Yea JW, Kang MK. Fabrication of malleable three-dimensional-printed customized bolus. *PLoS One* 2017; 12: e0177562.
19. Scarboro SB, Cody D, Stingo FC, Alvarez P, Followill D, Court L, et al. Calibration strategies for use of nanoDot OSLD in CT applications. *J Appl Clin Med Phys* 2019; 20: 331-339.
20. Yukihara EG, Bos AJJ, Bilski P, McKeever SWS. The quest for new thermoluminescence and optically stimulated luminescence materials. *Radiat Meas* 2022; 158: 106846.
21. Mizuno H, Fukumura A, Fukahori M, Sakata S, Yamashita W, Takase N, et al. Application of a radiophotoluminescent glass dosimeter to nonreference condition dosimetry. *Med Phys* 2014; 41: 112104.
22. Erdogan T, Fidan U, Ozyigit G. Patient-specific tumor and respiratory monitoring phantom design for SABR quality control. *Phys Med* 2021; 90: 40-49.
23. Araki F, Ohno T. Response of a radiophotoluminescent glass dosimeter in megavoltage beams. *Med Phys* 2014; 41: 122102.
24. Ma CM, Jiang SB, Pawlicki T, Chen Y, Li JS, Deng J, et al. A quality assurance phantom for IMRT dose verification. *Phys Med Biol* 2003; 48: 561-577.
25. Kry SF, Howell RM, Followill DS, et al. The use of 3D printing in radiation oncology. *Med Phys* 2020; 47: e745-e758.
26. Ehler J, Barney SN, Higgins AK, et al. Characterization of 3D printing materials for anthropomorphic phantoms. *Med Phys* 2014; 41: 071702.